Journal of Luminescence 201 (2018) 255–264

Contents lists available at ScienceDirect

Journal of Luminescence

journal homepage: www.elsevier.com/locate/jlumin

Lanthanide-doped disordered crystals: Site symmetry and optical properties

Wenwu You[a,b], Datao Tu[a,*], Wei Zheng[a], Ping Huang[a], Xueyuan Chen[a,b,**]

[a] CAS Key Laboratory of Design and Assembly of Functional Nanostructures, Fujian Key Laboratory of Nanomaterials, and State Key Laboratory of Structural Chemistry, Fujian Institute of Research on the Structure of Matter, Chinese Academy of Sciences, Fuzhou, Fujian 350002, China
[b] University of Chinese Academy of Sciences, Beijing 100049, China

ARTICLE INFO

Keywords:
Site symmetry
Disordered crystals
Lanthanide ions
Downshifting
Upconversion

ABSTRACT

Lanthanide ions (Ln^{3+}) doped disordered crystals, which exhibit excellent downshifting/upconversion luminescent properties, are widely used in a variety of optical and optoelectronic fields. The optical properties of Ln^{3+} ions are critically dependent on the local structure around Ln^{3+} ions. Therefore, by employing Ln^{3+} (*e.g.*, Eu^{3+}) as the sensitive structural probe, the local structure and site symmetry of Ln^{3+} dopants in the disordered crystals can be determined. Furthermore, through modification of the local site symmetry of Ln^{3+} ions, various highly efficient Ln^{3+}-doped luminescent materials have been designed over the past decade. As such, it is urgent to renew the knowledge about the huge family of Ln^{3+}-doped disordered crystals. Rather than being exhaustive, this review aims to highlight the most recent advances in the site symmetry and optical properties of Ln^{3+}-doped disordered crystals, with an emphasis on probing the local site symmetry and tuning downshifting/upconversion luminescent properties based on modification of the microstructures around Ln^{3+} dopants. Finally, the challenges and future perspectives of this important kind of phosphors are proposed.

1. Introduction

Disordered crystals, in which two or more cations statistically occupy the same lattice site, are frequently employed as hosts for doping with lanthanide or transition metal ions [1–9]. Specifically, trivalent lanthanide ion (Ln^{3+}) doped disordered crystals such as $AREF_4$ (A = K, Na; RE = rare earth), $AB(XO_4)_2$ (A = Li, Na; B = rare earth or Bi; X = Mo, W), MF_2 (M = Ca, Sr, Ba), garnets and apatites have gained much research interest and been widely used for anti-counterfeiting, imaging, lasers, and bioassays due to their excellent downshifting (DS) and upconversion (UC) luminescent properties [10–38].

The DS/UC luminescent properties of Ln^{3+} ions depend critically on their site symmetry, and a small difference in the local site symmetry might lead to significant change in electronic energy levels and excited-state dynamics of doped Ln^{3+} ions [39,40]. Generally, it is difficult to identify the actual local site symmetry in disordered crystals *via* traditional diffraction methods, because these methods usually take into account cations randomly occupying the same lattice site as a virtual "average" ion according to their respective probabilities [41]. Fortunately, Ln^{3+} ions such as Eu^{3+} can be employed as sensitive structure probes to reveal the local site symmetry [42,43]. The excited state ($^5D_0$) and the ground state ($^7F_0$) of Eu^{3+} ion are non-degenerate and will not be split by the crystal-field (CF) effect. Therefore, Eu^{3+} with different local symmetry possesses different $^5D_0$ and $^7F_0$ states, and the number of $^5D_0 \rightarrow {}^7F_0$ transition lines can be used to identify the multiple Eu^{3+} sites in the hosts. In addition, according to the electric dipole (ED) selection rule, the transition between $^5D_0$ and $^7F_0$ is only observed in the emission spectrum in the following 10 site symmetries without inversion symmetry: C_s, C_1, C_2, C_3, C_4, C_6, C_{2v}, C_{3v}, C_{4v}, and C_{6v}, respectively [42,44]. Furthermore, the $^5D_0 \rightarrow {}^7F_2$ transition of Eu^{3+} is an ED transition that is highly sensitive to the local site symmetry, while the $^5D_0 \rightarrow {}^7F_1$ transition is a magnetic dipole (MD) transition that is insensitive to its local site symmetry. As such, the intensity ratio of the $^5D_0 \rightarrow {}^7F_2$ transition to the $^5D_0 \rightarrow {}^7F_1$ transition of Eu^{3+} is closely related to the site symmetry [42]. Based on the Judd–Ofelt (JO) theory and the selection rules of *f-f* transitions, the number of allowed transition lines between $^5D_0 \rightarrow {}^7F_J$ (J = 0, 1, 2, 3, 4, 5 and 6) of Eu^{3+} at 32 crystallographic point groups is summarized in Table 1 [45]. Accordingly, the local site symmetry can be determined by comparing the numbers of the experimental $^5D_0 \rightarrow {}^7F_J$ transitions lines with the number of theoretically allowed transition lines [46]. In most cases, the symmetry of spectroscopic sites for Ln^{3+} ions in disordered crystals (*e.g.*, $NaYF_4$, $NaGd(WO_4)_2$, $NaLa(MoO_4)_2$) was observed to deviate from that of crystallographic sites [46–51].

* Corresponding author.
** Corresponding author at: CAS Key Laboratory of Design and Assembly of Functional Nanostructures, Fujian Key Laboratory of Nanomaterials, and State Key Laboratory of Structural Chemistry, Fujian Institute of Research on the Structure of Matter, Chinese Academy of Sciences, Fuzhou, Fujian 350002, China.
E-mail addresses: dttu@fjirsm.ac.cn (D. Tu), xchen@fjirsm.ac.cn (X. Chen).

https://doi.org/10.1016/j.jlumin.2018.04.057
Received 12 February 2018; Accepted 26 April 2018
Available online 03 May 2018

Table 1
Theoretically allowed transition lines of $^5D_0 \rightarrow {}^7F_J$ of Eu^{3+} ions at 32 crystallographic point groups. (Adapted with permission from Ref. [45]. Copyright 2009, American Chemical Society).

Crystal system	Symmetry	The number of allowed transition lines of $^5D_0 \rightarrow {}^7F_J$						
		$J = 0$	1	2	3	4	5	6
Triclinic	C_1	1	3	5	7	9	11	13
	C_i	0	3	0	0	0	0	0
Monoclinic	C_s	1	3	5	7	9	11	13
	C_2	1	3	5	7	9	11	13
	C_{2h}	0	3	0	0	0	0	0
Orthorhomic	C_{2v}	1	3	4	5	7	8	10
	D_2	0	3	3	6	6	9	9
	D_{2h}	0	3	0	0	0	0	0
Tetragonal	C_4	1	2	2	3	5	6	6
	C_{4v}	1	2	2	2	4	4	5
	S_4	0	2	3	4	4	5	7
	D_{2d}	0	2	2	3	3	4	5
	D_4	0	2	1	3	3	5	4
	C_{4h}	0	2	0	0	0	0	0
	D_{4h}	0	2	0	0	0	0	0
Trigonal	C_3	1	2	3	5	6	7	9
	C_{3v}	1	2	3	3	5	5	7
	D_3	0	2	2	4	4	6	6
	D_{3d}	0	2	0	0	0	0	0
	S_6	0	2	0	0	0	0	0
Hexagonal	C_6	1	2	2	2	2	3	5
	C_{6v}	1	2	2	1	2	2	4
	D_6	0	2	1	2	1	3	3
	C_{3h}	0	2	1	3	4	4	4
	D_{3h}	0	2	1	2	3	3	3
	C_{6h}	0	2	0	0	0	0	0
	D_{6h}	0	2	0	0	0	0	0
Cubic	T	0	1	1	2	2	3	3
	T_d	0	1	1	1	1	1	2
	T_h	0	1	0	0	0	0	0
	O	0	1	0	1	1	2	1
	O_h	0	1	0	0	0	0	0

The unique disordered structure is benificial for efficient energy transfer among Ln^{3+} dopants, which makes Ln^{3+}-doped disordered crystals an excellent kind of phosphors for various applications. In order to improve their photoluminescence (PL) efficiency and tune the optical performance, different synthesis approaches together with some complementary strategies for modification of the local structure have been proposed [52–54]. Currently, three main strategies are generally applied to modulate the local microstructure around Ln^{3+} dopants (Fig. 1). The first strategy is codoping Ln^{3+} with homovalent ions, in which the crystal lattice contract or expand due to the mismatch of ionic radius between codoped ions and host lattice ions. The second one is codoping Ln^{3+} with heterovalent ions, in which vacancies or interstitial ions are introduced into the host lattices due to the requirement of charge compensation. The third one is engineering composition of the host. Different from homovalent or heterovalent ions codoping strategies, no impurity ions were introduced in the host. Nevertheless, the introduced vacancies through composition engineering may also change the local structure around Ln^{3+} dopants.

In the past few years, several excellent reviews on the topic of Ln^{3+}-doped inorganic materials have been published [55–61]. However, most of them focused on the chemical synthesis, optical properties designing and diverse applications. To the best of our knowledge, there is no review focusing on the site symmetry and optical properties of Ln^{3+}-doped disordered crystals. In this review, we aim to elucidate the relationship between local site symmetry and the optical properties of these Ln^{3+}-doped disordered phosphors, and to provide the readers with inspiring ideas for tuning the PL properties of Ln^{3+}-doped disordered crystals (Fig. 1). To begin with, we briefly describe the crystallographic and spectroscopic site symmetry of Ln^{3+} in disordered crystals (Section 2), with an emphasis on probing the local site symmetry of typical Ln^{3+}-doped disordered crystals such as $NaREF_4$ (RE: rare earth), $NaRE(WO_4)_2$ and $NaRE(MoO_4)_2$. We then highlight three main strategies for tuning the DS/UC luminescence of Ln^{3+}-doped crystals based on modification of the local site symmetry of Ln^{3+} ions (Section 3). Finally, some future prospects and efforts toward this active

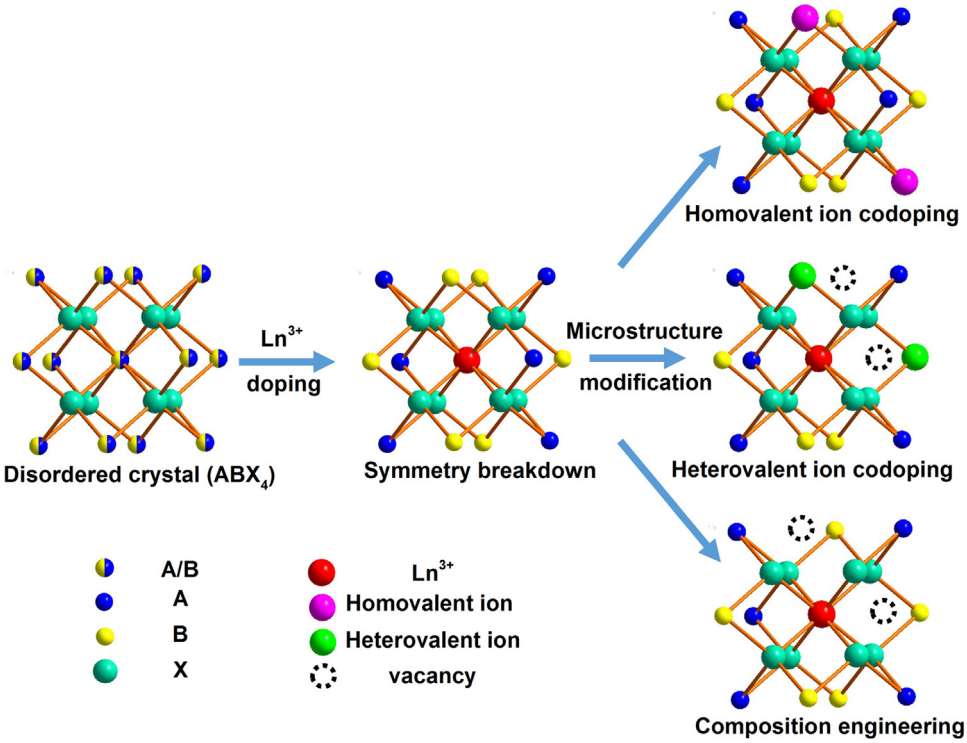

Fig. 1. Schematic illustration of symmetry breakdown in Ln^{3+}-doped disordered crystals and three main strategies to modulate the local microstructure in disordered crystals.

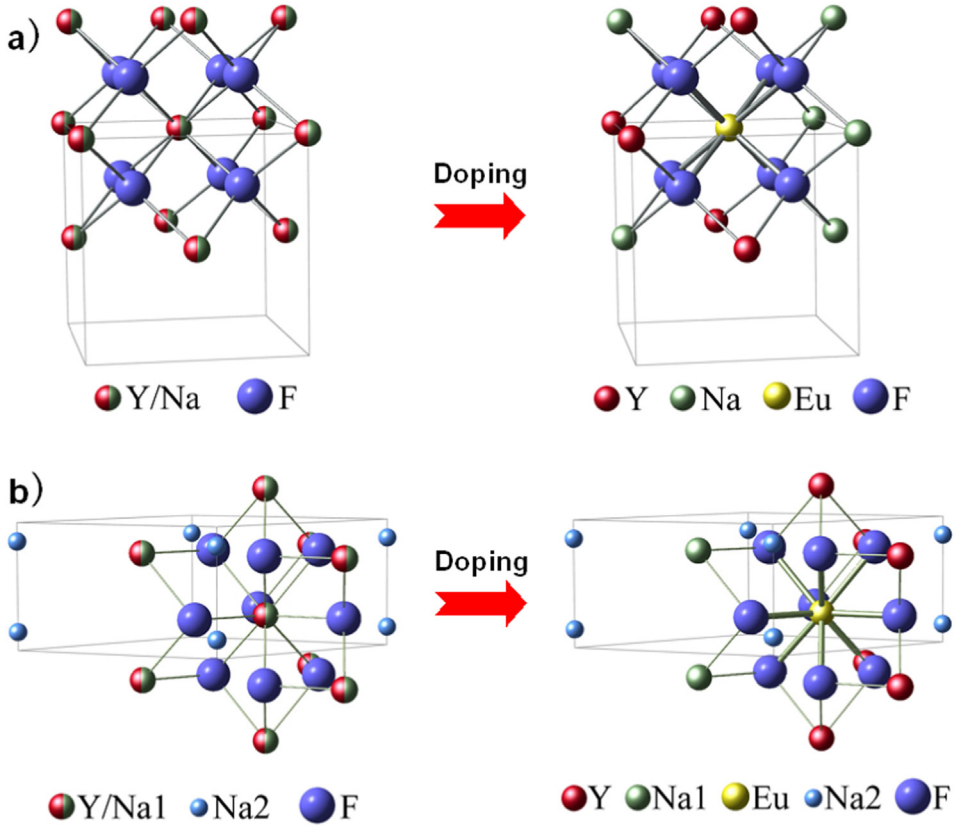

Fig. 2. Schematic illustration showing the breakdown of the crystallographic site symmetry of Eu^{3+} in (a) cubic and (b) hexagonal $NaYF_4$ crystals. Induced by Eu^{3+}-doping for the disordered Y/Na site, the original crystallographic site symmetries of O_h in (a) and C_{3h} in (b) may descend to C_s and C_s, respectively. (Adapted with permission from Ref. [46]. Copyright 2013, John Wiley & Sons, Inc.).

research field are proposed.

2. Site symmetry of Ln^{3+} in disordered crystals

2.1. Crystallographic site symmetry

The crystal structure of luminescent materials can be revealed by traditional diffraction methods. Note that such standard crystallography analysis takes into account those ions randomly occupying the same lattice site as a virtual "average" ion. As a result, the cations statistically occupying the same lattice site are identified with the same site symmetry [41,46]. For example, $NaYF_4$ is regarded as one of the most efficient host material for doping with Ln^{3+} ions to produce intense green (doped with Yb^{3+}/Er^{3+}) and blue (doped with Yb^{3+}/Tm^{3+}) UC emission [62]. $NaYF_4$ usually exists in two phase structures: cubic and hexagonal. Both cubic and hexagonal $NaYF_4$ are disordered crystals, in which Na^+ and Y^{3+} are statistically distributed over the same lattice site with space groups of *Fm-3m* and $P6_3/m$, respectively (Fig. 2) [63]. From single-crystal XRD data, the average structure of cubic $NaYF_4$ is a derivative CaF_2 fluorite type with the Ca^{2+} site randomly occupied by 1/2 Na^+ and 1/2 Y^{3+}. The crystallographic symmetry of both Na^+ and Y^{3+} are determined to be O_h. For hexagonal $NaYF_4$, one kind of nine-fold coordinated cation site is randomly occupied by 1/4 Na^+ and 3/4 Y^{3+} with crystallographic site symmetry of C_{3h} [46]. When Ln^{3+} (*e.g.*, Eu^{3+}) ions are doped into cubic or hexagonal $NaYF_4$, in view of the different ionic radius between Ln^{3+} and Y^{3+}, the bond length of Ln-F will be different from that of Y-F. Consequently, such difference will perturb the coordination shell around the site originally randomly distributed by Y^{3+} and Na^+. According to the microscopic model displayed in Fig. 2, it is anticipated that the site symmetry of each subset of Ln^{3+} may be reduced from O_h in cubic $NaYF_4$ (or C_{3h} in hexagonal $NaYF_4$) to lower ones such as C_s or even C_1.

2.2. Spectroscopic site symmetry

It should be noted that the breakdown of crystallographic site symmetry is a universal phenomenon in Ln^{3+}-doped disordered crystals, which can be verified by the high-resolution PL spectra of Ln^{3+}. To date, a series of Ln^{3+}-doped disordered crystals such as fluorides, garnets, apatites, molybdates, borates, vanadates, tungstates, langasites, and langatates have been reported [37,38,64–71]. Among these disordered crystals, $NaREF_4$ has received great attention during the past years, due to their low phonon frequencies, high chemical stability and high UC luminescence efficiency [72–76].

Recently, our group provided solid spectroscopic evidence to verify the breakdown of crystallographic site symmetry in Ln^{3+}-doped cubic and hexagonal $NaYF_4$ crystals by means of 10 K high-resolution site-selective excitation and emission spectroscopy of Eu^{3+} ions [46]. Only one site of Eu^{3+} was observed in Eu^{3+} doped cubic and hexagonal $NaYF_4$ crystals, respectively. The number of $^5D_0 \rightarrow {}^7F_{0,1,2}$ emission lines in the emission spectrum of Eu^{3+}-doped hexagonal $NaYF_4$ are 1, 3 and 5, respectively, which verified that the site symmetry of Eu^{3+} descend from C_{3h}, to C_s according to the branching rules (Fig. 3) and transition selection rules of the 32 point groups (Table 1) [45,77]. Similarly, the site symmetry of Eu^{3+} in cubic $NaYF_4$ crystals was found to descend from O_h to C_s or C_2. Such site symmetry breakdown from their crystallographic site symmetry was also observed in other disordered crystals like cubic $KLaF_4$ and $KGdF_4$ by employing Eu^{3+} as structure probe (Fig. 4) [44,78]. In the 10 K emission spectra, both the number of $^5D_0 \rightarrow {}^7F_{0,1,2}$ emission lines of Eu^{3+} were observed to be 1, 3 and 5, respectively (Fig. 4). Thus, the highest site symmetry of Eu^{3+} in cubic $KLaF_4$ and $KGdF_4$ crystals was determined to be C_s or C_2.

Besides the families of $NaREF_4$ and $KREF_4$, similar symmetry breakdown also occurred in other kinds of disordered crystals like double molybdates and tungstates, with general formula of $AB(XO_4)_2$ (A = Li, Na; B = RE, Bi and X = Mo, W). These crystals belong to tetragonal scheelite ($CaWO_4$) structure, where A^+ and B^{3+} ions occupy

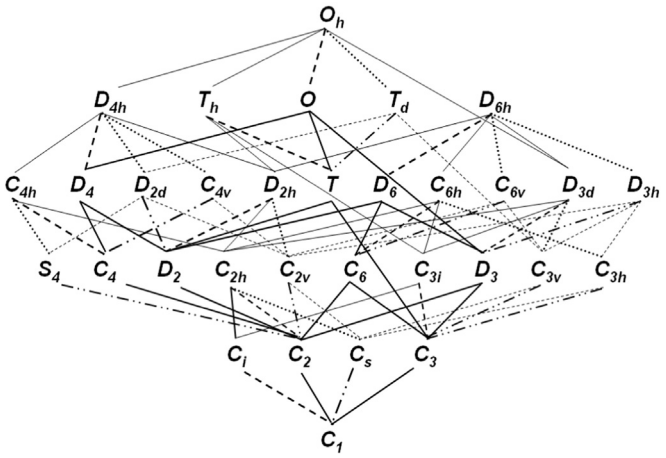

Fig. 3. Branching rules of the 32 point groups. (Adapted with permission from Ref. [77]. Copyright 1981, Plenum Press, New York.).

the site of Ca^{2+} with site symmetry of S_4 [35]. In an effort to identify the site symmetry of Ln^{3+} dopants in $AB(XO_4)_2$, Wang and co-workers synthesized Eu^{3+} doped $NaLu(WO_4)_2$ red-emitting phosphor [79]. Upon excitation at 395 nm, the 10 K high-resolution PL emission spectrum of Eu^{3+} was obtained, which consists of a series of resolved bands from 500 to 750 nm (Fig. 5). In principle, Eu^{3+} ions substituting Lu^{3+} ions in $NaLu(WO_4)_2$ possess a crystallographic site with point-group symmetry of S_4. The number of the $^5D_0 \rightarrow {}^7F_{0,1,2}$ emission lines should be 0, 2 and 3, respectively. However, the intensity of the $^5D_0 \rightarrow {}^7F_2$ transition (ED transition) is much higher than that of the $^5D_0 \rightarrow {}^7F_1$ transition (MD transition). In addition, the appearance of the $^5D_0 \rightarrow {}^7F_0$ transition in the PL spectrum explicitly verified the low site symmetry of Eu^{3+} doped in $NaLu(WO_4)_2$. Specifically, the numbers of transition lines from $^5D_0$ to $^7F_0$, $^7F_1$ and $^7F_2$ are 1, 3, 5, respectively. Therefore, the highest site symmetry of Eu^{3+}, distorted from S_4, should be C_2.

3. Modification of microstructures in disordered crystals

In order to improve the PL efficiency of Ln^{3+}-doped disordered crystals for various applications, conventional strategies such as selection of host matrices, designing of core/shell structure and optimization of the Ln^{3+} concentration are frequently adopted [80–83]. Because the optical properties of Ln^{3+} ions are dependent on their local structure, modification of the microstructure of Ln^{3+} dopants in disordered crystals enables regulation of the optical performance of Ln^{3+}-doped disordered crystals. To this end, several approaches like cation (homovalent or heterovalent ions) codoping with Ln^{3+}, and host composition engineering have emerged as effective routes for the synthesis of highly efficient Ln^{3+}-doped disordered phosphors [54,84–90], as will be briefly overviewed in this section.

3.1. Microstructure of disordered crystals

When Ln^{3+} ions are doped in disordered crystals, the minute structural distortion induces a locally variable CF surrounding around the dopants. For each subset of Ln^{3+} ions, the CF surrounding might be slightly different. Consequently, the line-widths of the electronic transitions (absorption and emission bands) for whole set of Ln^{3+} are found to be inhomogeneously broadened relative to that in ordered crystals [36,91,92]. Previously, such inhomogeneously broadened spectra of Ln^{3+} emitters including Eu^{3+}, Nd^{3+} and Yb^{3+} were observed in a variety of disordered crystals [46,93,94]. For example, the full width at half maximum (FWHM) of the $^5D_0 \rightarrow {}^7F_0$ transition of Eu^{3+} at 10 K in cubic $NaYF_4$ is ~ 1.3 nm, which is much broader than that of Eu^{3+} in ordered crystals (FWHM is ~ 0.1 nm) [46]. Likewise, inhomogeneous broadening of the absorption and emission bands was often reported in Ln^{3+}-doped disordered laser crystals like $Sr_3Y(BO_3)_3$, $Li_2Gd_4(MoO_4)_7$ and $SrGdGa_3O_7$, to name a few [95–97]. The broad absorption linewidths of the Ln^{3+} activators doped in disordered crystals make them very suitable for diode pumping, whereas the broad emission bands of the activators enable them for potential laser applications such as tunable or short pulse lasers [94].

Besides the applications in laser, the disordered structure may favor the UC population due to efficient energy transfer among Ln^{3+} dopants in disordered crystals. In 2011, Renero-Lecuna and co-workers demonstrated that the high UC efficiency in hexagonal $NaYF_4$:Er^{3+}/Yb^{3+} crystal was due mainly to the ideal resonance conditions of the energy transfer from Yb^{3+} to Er^{3+} among multisites [7]. As shown in Fig. 6, a series of distinct emission spectra were observed upon excitation at different wavelengths between 482 and 488 nm. The slight spectral variations and the peak shifts observed in each emission spectrum revealed the existence of multisite Er^{3+} dopants in the host, which were also confirmed by their distinct pressure-dependent room-temperature UC emission patterns. Similarly, multiple sites of Ln^{3+} in disordered $NaLaF_4$ crystals were observed by Sarakovskis and co-workers [98]. In their work, at least three different kinds of Er^{3+} ions with different CF environments were identified *via* site-selective spectroscopy. Moreover, efficient energy transfer between Er^{3+} at different sites was confirmed both in the UC and DS luminescent processes, which thus well interpreted the high PL efficiency of Er^{3+} in such disordered crystals.

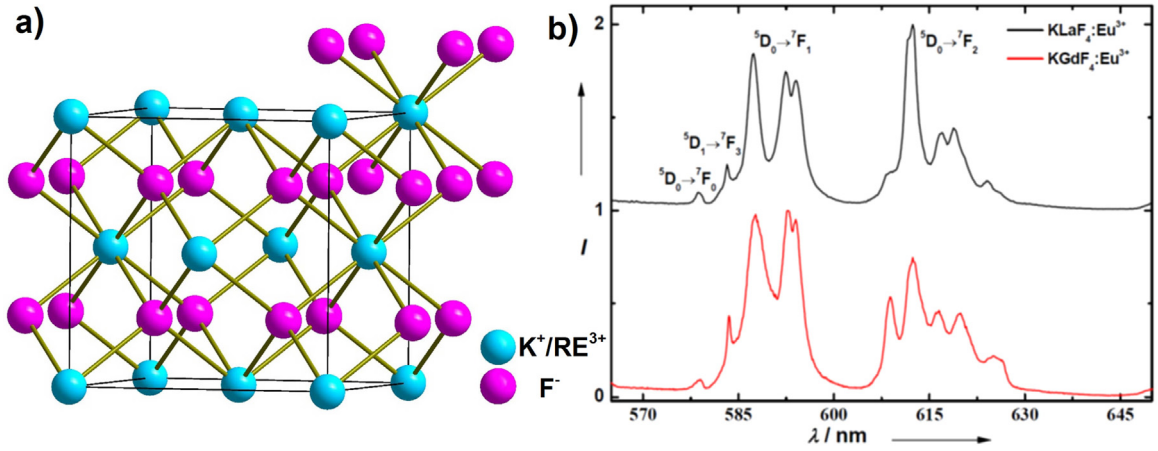

Fig. 4. (a) Schematic illustrations showing the crystal structures of cubic $KREF_4$, the crystallographic site symmetry of RE^{3+} is O_h. (b) 10 K emission spectra of cubic $KLaF_4$:Eu^{3+} (5 mol%) and $KGdF_4$:Eu^{3+} (5 mol%) crystals upon excitation at 394 nm. (Adapted with permission from Ref. [46]. Copyright 2013, John Wiley & Sons, Inc.).

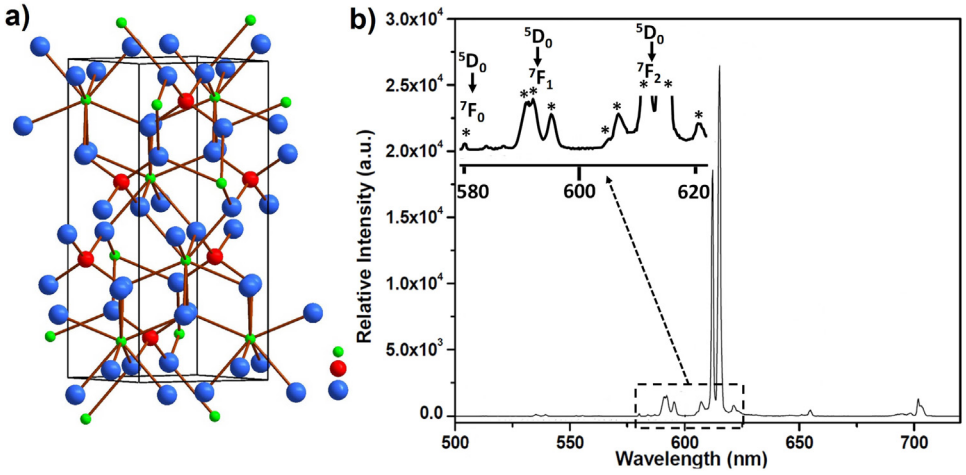

Fig. 5. (a) Schematic illustrations showing the crystal structure of $NaRE(WO_4)_2$, in which the crystallographic site symmetry of RE^{3+} is S_4. (b) 10 K emission spectrum of $NaLu(WO_4)_2:Eu^{3+}$ upon excitation at 395 nm. The inset shows the ten-fold magnified emission spectrum in the range from 580 nm to 621 nm. Peaks corresponding to the $^5D_0 \rightarrow {}^7F_{0,1,2}$ transitions are marked as star symbols. (Adapted with permission from Ref. [79]. Copyright 2013, Optical Society of America.).

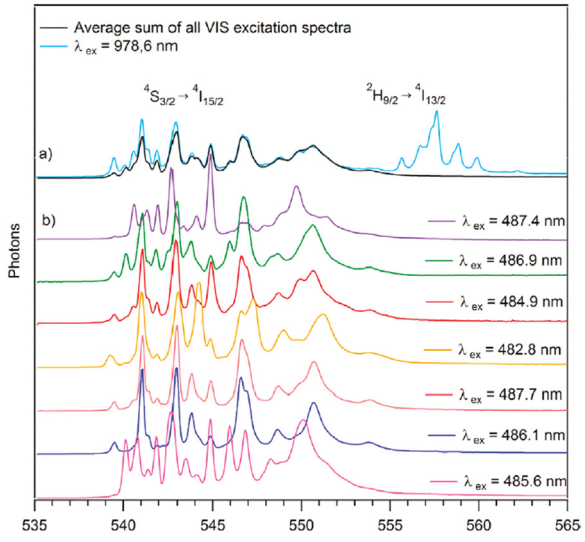

Fig. 6. Emission spectra of hexagonal $NaYF_4:Er^{3+}/Yb^{3+}$ upon excitation at different excitation wavelengths (482–488 nm) at 17 K. (Adapted with permission from Ref. [7]. Copyright 2011, American Chemical Society.).

3.2. Homovalent ions codoping with Ln^{3+} ions

Impurity doping, which has significant influence on the nucleation and growth of many nanomaterials, is often proposed as the main approach to modify the crystallographic phase, size, shape and electronic configuration of crystals [52,63,85].

By codoping Ln^{3+} with homovalent (trivalent) ions, the host lattice might expand or contract when large- or small-size impurity ions are doped to substitute the host cations. To exemplify this, Wang and co-workers demonstrated that Gd^{3+} doping can dramatically influence the growth process of $NaYF_4:Yb^{3+}/Er^{3+}$ nanocrystals (NCs) [63]. In their work, simultaneous controlling of the crystallographic phase, size and UC properties of $NaYF_4:Yb^{3+}/Er^{3+}$ NCs was realized. Without the introduction of Gd^{3+} ions, both small cubic nanocubes and large hexagonal nanorods were obtained in aqueous solvent at 200 °C for 2–10 h (Fig. 7a–c). After codoping with Gd^{3+} (30, 45, 60 mol%), the cubic-to-hexagonal phase conversion happened after only 2 h (Fig. 7d–f). With increasing the content of Gd^{3+}, hexagonal-phase nanorods with smaller size were synthesized. Density functional theory (DFT) calculations indicated that the formation energy per atom in hexagonal $NaYF_4$ increased by ~ 0.07 eV when Y^{3+} was replaced by Gd^{3+}. Therefore, $NaGdF_4$ should be more energetically stable than $NaYF_4$. Increasing the Gd^{3+} content in $NaYF_4$ host matrix facilitated the formation of hexagonal-phase NCs. Subsequently, Wisser and co-workers prepared Gd^{3+} and Lu^{3+} codoped hexagonal $NaYF_4$ NCs [52]. The UC quantum yield for hexagonal $NaYF_4:Yb^{3+}/Er^{3+}$ was determined to be 0.045%. After Gd^{3+} and Lu^{3+} codoping, a maximum UC quantum yield of 0.074% was achieved for hexagonal $NaY_{.72}Gd_{.04}Lu_{0.04}F_4$:Yb/Er NCs. The improvement of UC quantum yield is attributed to the increased radiative transition rates for Yb^{3+} and Er^{3+}, due to the local symmetry distortion in $NaY_{0.72}Gd_{0.04}Lu_{0.04}F_4$:Yb/Er NCs. Till now, a number of trivalent ions like Al^{3+}, Y^{3+}, La^{3+}, Gd^{3+}, Bi^{3+}, Mo^{3+}, Fe^{3+}, and Sc^{3+} have been exploited to modulate the microstructure of disordered crystals (Table 2) [5,84,85,90,99–107].

Besides modulation of microstructure of the host lattice, the codoping of homovalent (trivalent) ions with Ln^{3+} may modulate the distance between Ln^{3+} emitters in disordered crystals. For instance, the codoping of Yb^{3+} or Lu^{3+} ions in $CaF_2:Pr^{3+}$ crystals was demonstrated to avoid the clustering of Pr^{3+} ions [108]. In $CaF_2:Pr^{3+}/Lu^{3+}$, Pr^{3+}-Pr^{3+} clusters were replaced by Pr^{3+}-Lu^{3+} clusters. An enhanced PL intensity of Pr^{3+} by a factor of 500 can be achieved in $CaF_2:Pr^{3+}/Lu^{3+}$ relative to that of $CaF_2:Pr^{3+}$, due to the decreased nonradiative relaxation rate between Pr^{3+} ions. Moreover, the formation of Pr^{3+}-Yb^{3+} clusters in place of Pr^{3+}-Pr^{3+} clusters may lead to highly efficient energy transfer from Pr^{3+} to Yb^{3+} with an ultrafast rate of $5 \times 10^7\ s^{-1}$. The $^3P_0$ lifetime of Pr^{3+} was determined to be 150 μs in $CaF_2:Pr^{3+}$, but only 1.3 μs in $CaF_2:Pr^{3+}/Yb^{3+}$(0.5%/10%). The energy transfer efficiency (E) was calculated to be 99.1%, according to the formula $E = (\tau_0-\tau_1)/\tau_0$, where τ_0 and τ_1 are the donor lifetime in the absence and presence of acceptor, respectively [109].

3.3. Codoping Ln^{3+} with heterovalent ions

The strategy of codoping Ln^{3+} with heterovalent (monovalent, divalent or tetravalent) ions is proposed as an alternative way to modify the microstructure or regulate their optical performance in the disordered NCs (Table 3) [53,86–90,110–120]. Different from homovalent codoping, heterovalent codoping usually introduces interstitial ions (or extra vacancies) into the host matrix during the nucleation and growth processes, due to the requirement of charge compensation. Correspondingly, the PL properties of Ln^{3+} can be tuned by codoping with different cation content. As reported by Zhao and co-workers, the introduction of 13.5 mol% Mg^{2+} ions in $NaGdF_4:Yb^{3+}/Er^{3+}$ NCs resulted in 9, 6, and 7 times enhancement of the red, green and violet UC emission, respectively [115]. More significant enhancement effects were realized in Ca^{2+}-codoped $NaGdF_4:Yb^{3+}/Er^{3+}$ NCs by Lei and co-workers [88]. With increasing the Ca^{2+} content, the morphology of $NaGdF_4$ NCs changed from irregular shape to hexagonal plates, and finally to uniform nanorods. When codoping with 30 mol% Ca^{2+} in $NaGdF_4:Yb^{3+}/Er^{3+}$ NCs, the UC emission intensity of Er^{3+} was

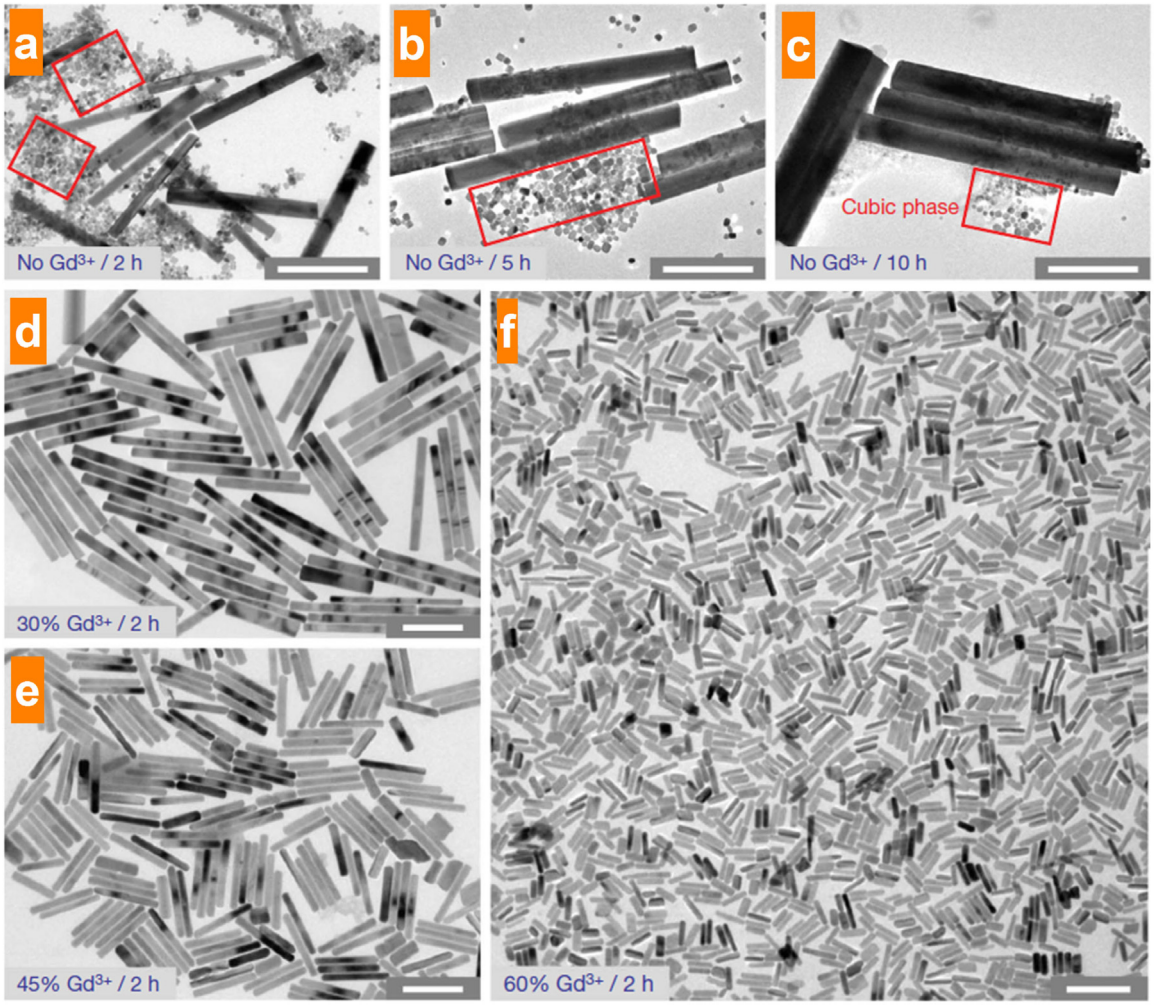

Fig. 7. (a–c) TEM images of $NaYF_4$:Yb^{3+}/Er^{3+} (18/2 mol%) NCs obtained after heating for 2, 5 and 10 h at 200 °C without the codoping of Gd^{3+} ions. Formation of the cubic $NaYF_4$ is partially marked by red squares. (d–f) TEM images of $NaYF_4$:Yb^{3+}/Er^{3+} (18/2 mol%) NCs obtained after heating for 2 h at 200 °C with the codoping of 30, 45 and 60 mol% Gd^{3+} ions, respectively. Scale bars are 500 nm for panels a–c, 200 nm for panels d–f. (Adapted with permission from Ref. [63]. Copyright 2010, Nature Publishing Group.).

enhanced by a factor of ~ 200 times (Fig. 8a). They attributed the enhanced UC emission to the modification of the crystal microstructure of $NaGdF_4$ NCs after codoping Ca^{2+} ions (Fig. 8b). Similarly, codoping with other divalent ions (*e.g.*, Sr^{2+}, Ba^{2+}, Zn^{2+}, Mg^{2+}, Co^{2+}) or tetravalence ions (*e.g.*, Ti^{4+}, Sn^{4+}) proved to be an effective strategy for tuning the UC performance of $NaREF_4$ or $KREF_4$ NCs [88,115,116,118–121].

Among the heterovalent codoping, alkali metal ions are most frequently introduced into disordered crystals to regulate their optical performance [53,86,87,89,90,110,111,113,114,117,122,123]. For example, we recently reported that Na^+ ions doping was able to significantly improve the crystallinity of the ultrasmall CaF_2:Ln^{3+} NCs as well as their PL intensity [117]. By measuring the PL spectra and PL decays of CaF_2:Ce^{3+}/Tb^{3+} and CaF_2:Ce^{3+}/Tb^{3+}/Na^+ NCs, we provided solid spectroscopic evidence for the modification of CF in CaF_2:Ce^{3+}/Tb^{3+} NCs *via* Na^+ doping (Fig. 9). Specifically, the spectral

Table 2
PL enhancement of Ln^{3+}-doped disordered crystals by codoping with trivalent ions.

Host	Doped ions	Co-doped ions	Transitions	Wavelength (nm)	Times of PL enhancement	Ref.
$NaYF_4$	Yb^{3+}/Er^{3+}	Sc^{3+}	Er^{3+}: $^2H_{9/2}\rightarrow{}^4I_{15/2}$ $^2H_{11/2}/{}^4S_{3/2}\rightarrow{}^4I_{15/2}$ $^4F_{9/2}\rightarrow{}^4I_{15/2}$	400–420 510–570 630–700	5.0	[101]
$NaYF_4$	Yb^{3+}/Tm^{3+}	Sc^{3+}	Tm^{3+}: $^1G_4\rightarrow{}^3H_6$	460–500	2.0	[90]
$NaLuF_4$	Yb^{3+}/Er^{3+}	Y^{3+}	Er^{3+}: $^2H_{11/2}/{}^4S_{3/2}\rightarrow{}^4I_{15/2}$	510–570	1.8	[104]
$NaYbF_4$	Tm^{3+}	Gd^{3+}	Tm^{3+}: $^3H_4\rightarrow{}^3H_6$	750–850	17.0	[84]
$NaLuF_4$	Yb^{3+}/Er^{3+}	La^{3+}	Er^{3+}: $^4F_{9/2}\rightarrow{}^4I_{15/2}$	630–700	8.1	[100]
$NaYF_4$	Yb^{3+}/Er^{3+}	Bi^{3+}	Er^{3+}: $^2H_{9/2}\rightarrow{}^4I_{15/2}$ $^2H_{11/2}/{}^4S_{3/2}\rightarrow{}^4I_{15/2}$ $^4F_{9/2}\rightarrow{}^4I_{15/2}$	400–420 510–570 630–700	36.0	[5]
$NaGdF_4$	Yb^{3+}/Er^{3+}	Fe^{3+}	Er^{3+}: $^2H_{9/2}\rightarrow{}^4I_{15/2}$	400–420	12.0	[99]
$NaGdF_4$	Yb^{3+}/Er^{3+}	Mo^{3+}	Er^{3+}: $^2H_{11/2}/{}^4S_{3/2}\rightarrow{}^4I_{15/2}$	510–570	9.0	[106]
$KLaF_4$	Yb^{3+}/Er^{3+}	Al^{3+}	Er^{3+}: $^4F_{9/2}\rightarrow{}^4I_{15/2}$	630–700	7.3	[107]

Table 3
PL enhancement of Ln^{3+}-doped disordered crystals by codoping with heterovalent ions.

Host	Doped ions	Co-doped ions	Transitions	Wavelength (nm)	Times of PL enhancement	Ref.
$NaYF_4$	Yb^{3+}/Er^{3+}	Li^+	Er^{3+}: $^2H_{11/2}/^4S_{3/2}\rightarrow{}^4I_{15/2}$	510–570	9.5	[111]
CaF_2	Ce^{3+}/Tb^{3+}	Na^+	Tb^{3+}: $^5D_4\rightarrow{}^7F_J$	450–650	34.0	[117]
$NaYF_4$	Yb^{3+}/Tm^{3+}	K^+	Tm^{3+}: $^1G_4\rightarrow{}^3H_6$	460–500	4.0	[90]
$NaGdF_4$	Yb^{3+}/Er^{3+}	Ca^{2+}	Er^{3+}: $^2H_{9/2}\rightarrow{}^4I_{15/2}$	400–420	200	[88]
			$^2H_{11/2}/^4S_{3/2}\rightarrow{}^4I_{15/2}$	510–570		
			$^4F_{9/2}\rightarrow{}^4I_{15/2}$	630–700		
$NaYF_4$	Yb^{3+}/Er^{3+}	Zn^{2+}	Er^{3+}: $^2H_{11/2}/^4S_{3/2}\rightarrow{}^4I_{15/2}$	510–570	1.5	[116]
$NaGdF_4$	Yb^{3+}/Er^{3+}	Mg^{2+}	Er^{3+}: $^4F_{9/2}\rightarrow{}^4I_{15/2}$	630–700	9.0	[115]
$NaYF_4$	Yb^{3+}/Er^{3+}	Co^{2+}	Er^{3+}: $^2H_{9/2}\rightarrow{}^4I_{15/2}$	400–420	27.5	[118]
			$^2H_{11/2}/^4S_{3/2}\rightarrow{}^4I_{15/2}$	510–570		
			$^4F_{9/2}\rightarrow{}^4I_{15/2}$	630–700		
$NaYF_4$	Yb^{3+}/Er^{3+}	Sn^{4+}	Er^{3+}: $^2H_{11/2}/^4S_{3/2}\rightarrow{}^4I_{15/2}$	510–570	7.0	[119]
$NaYF_4$	Yb^{3+}/Er^{3+}	Ti^{4+}	Er^{3+}: $^2H_{9/2}\rightarrow{}^4I_{15/2}$	400–420	25.0	[120]
			$^2H_{11/2}/^4S_{3/2}\rightarrow{}^4I_{15/2}$	510–570		
			$^4F_{9/2}\rightarrow{}^4I_{15/2}$	630–700		

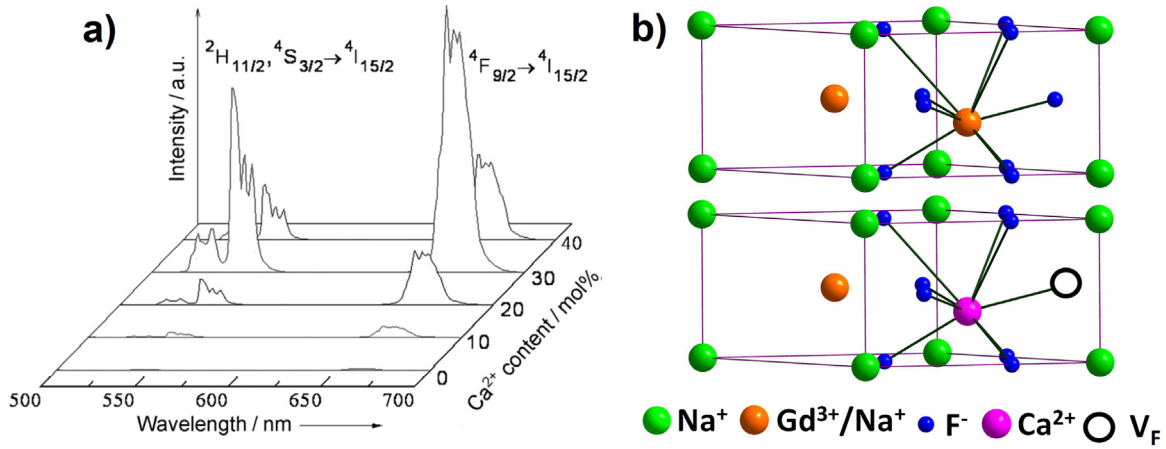

Fig. 8. (a) UC emission spectra of x% (x = 0, 10, 20, 30, 40) Ca^{2+} codoped $NaGdF_4$:Yb^{3+}/Er^{3+} NCs. (b) Schematic illustrations showing the crystal structure of $NaGdF_4$ without and with Ca^{2+} doping, respectively. (Adapted with permission from Ref. [88]. Copyright 2014, John Wiley & Sons, Inc.).

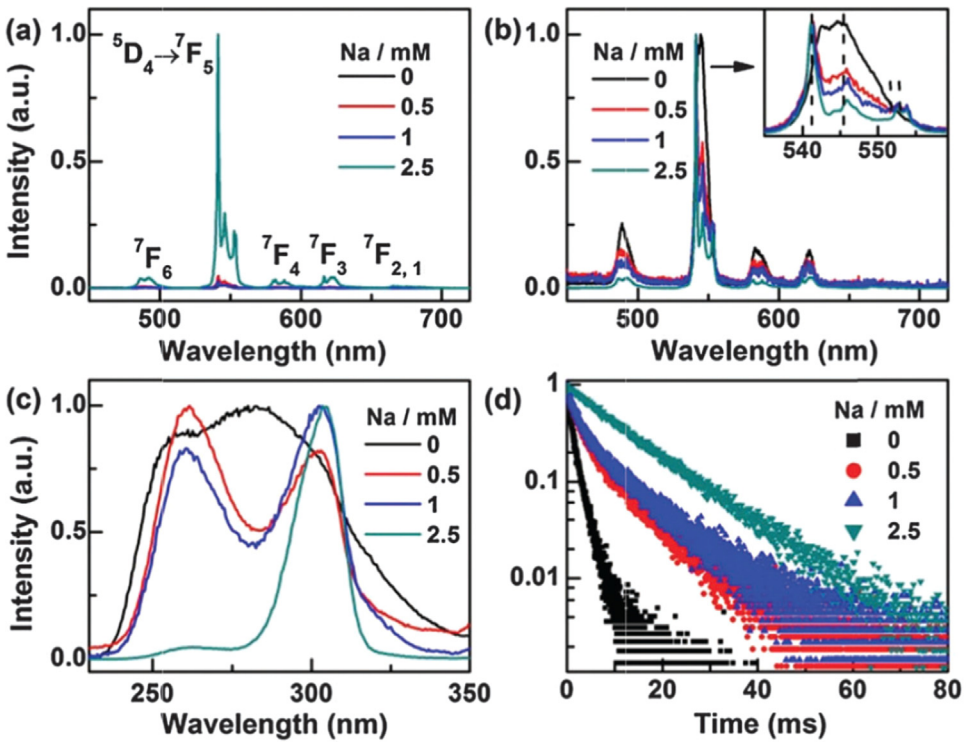

Fig. 9. (a) PL emission spectra and (b) the corresponding normalized emission spectra of CaF_2:5%Ce^{3+},5%Tb^{3+} NPs synthesized with different Na^+ concentrations upon excitation at 304 nm. The inset enlarges the spectral line splitting within 530–580 nm. (c) Normalized PL excitation spectra and (d) PL decay from $^5D_4$ by monitoring the Tb^{3+} emission at 541.2 nm for NPs synthesized with different Na + concentrations. (Adapted with permission from Ref. [117]. Copyright 2013, John Wiley & Sons, Inc.).

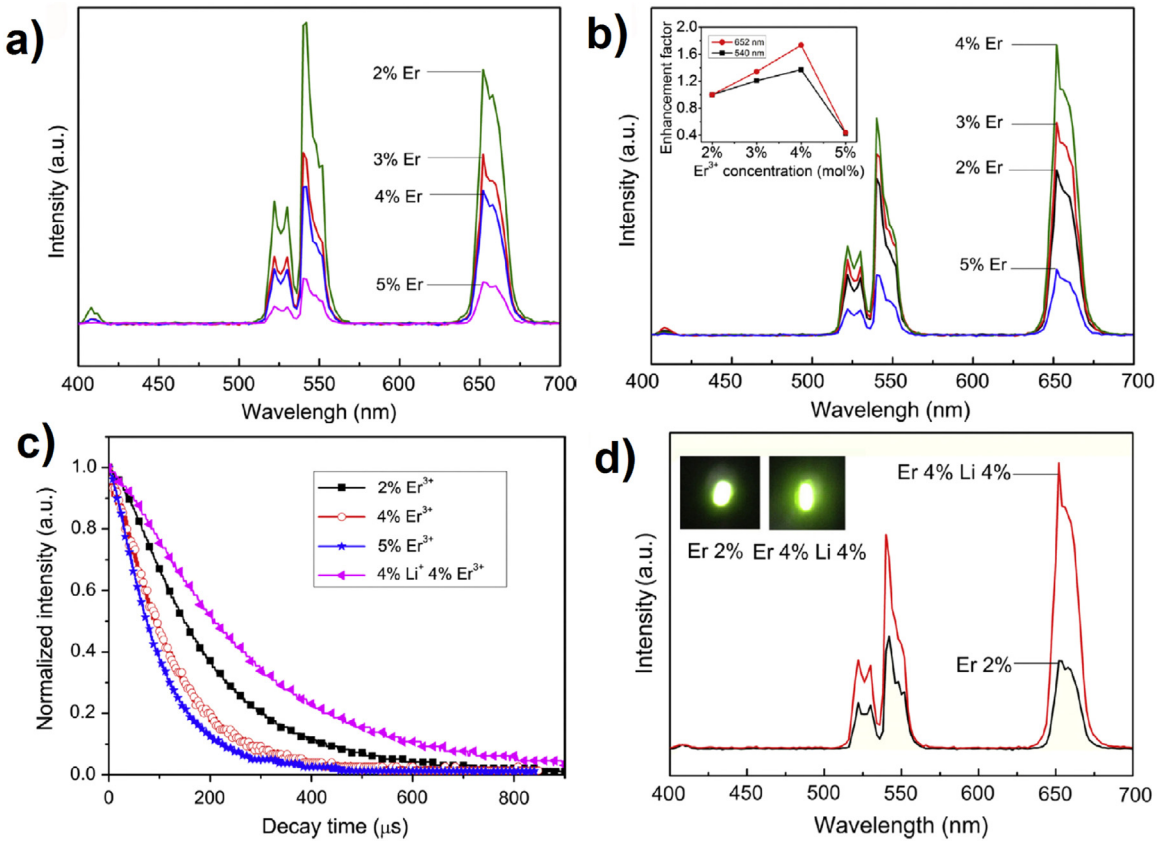

Fig. 10. Emission spectra of $NaYF_4$:18%Yb^{3+}/x%Er^{3+} (x = 2, 3, 4 and 5) (a) with and (b) with codoping 4 mol% Li^+. (c) PL decays from $^4S_{3/2}$ of Er^{3+} in $NaYF_4$:Yb^{3+}/Er^{3+} without and with codoping Li^+ ion. (d) Emission spectra of $NaYF_4$:18%Yb^{3+}/2%Er^{3+} and $NaYF_4$:18%Yb^{3+}/4%Er^{3+}/4%Li^+, respectively. (Adapted with permission from Ref. [89]. Copyright 2014, Elsevier.).

line splitting and the branching ratio of Tb^{3+}, the excitation band of Ce^{3+}, and the PL lifetime of Tb^{3+} varied significantly with the co-doping concentration of Na^+ (Fig. 9b-d). In comparison with Na^+-free CaF_2:Ce^{3+}/Tb^{3+} NCs, the PL intensity of CaF_2:Ce^{3+}/Tb^{3+}/Na^+ containing 2.5 mM Na^+ ions increased by 34 times (Fig. 9a). Correspondingly, the absolute PL quantum yield of CaF_2:Ce^{3+}/Tb^{3+} NCs increased from 9% to 51% after Na^+ doping. Besides, Ding and co-workers demonstrated that the doping of Li^+ can enhance the concentration quenching threshold in $NaYF_4$:Yb^{3+}/Er^{3+} [89]. As shown in Fig. 10a, without Li^+ codoping, the highest UC intensity of $NaYF_4$:18%Yb^{3+}/$x$$Er^{3+}$ (x = 2, 3, 4, 5) was observed at the Er^{3+} concentration of 2 mol %. However, the optimal Er^{3+} doping concentration was elevated to 4 mol% by codoping with 4 mol% Li^+ ion (Fig. 10b). In Li^+-codoped sample, Li^+ ions are supposed to separate the Er^{3+} clusters in the host and increase the distance between Er^{3+} ions, which thus reduce the nonradiative relaxation rate and increase the concentration quenching threshold. As a result, the PL lifetime of $^4S_{3/2}$ of Er^{3+} was prolonged after codoping with Li^+ (Fig. 10c). Meanwhile, the green and red UC emission intensity of $NaYF_4$:18%Yb^{3+}/4%Er^{3+}/4%Li^+ were 2 and 3.3 times stronger than that of $NaYF_4$:18%Yb^{3+}/2%Er^{3+} counterpart, respectively (Fig. 10d).

3.4. Engineering the host composition

Engineering the host composition is occasionally applied to tune the optical properties of Ln^{3+} in disordered crystals [54,124]. Recently, Dong and co-workers developed a facile and highly effective approach to tailor the UC emission by engineering the composition of cubic Na_xREF_{3+x} NCs. The local structure can be modified by precisely controlling the [Na]/[RE] and [F]/[RE] ratios (Fig. 11). As [Na]/[RE] (or [F]/[RE]) increased, the particle size became larger and the lattice

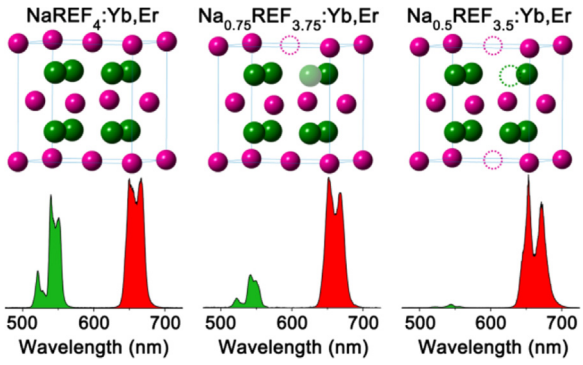

Fig. 11. Schematic illustration showing Na_xREF_{3+x} (x = 1, 0.75, 0.5) in a unit cell and the corresponding UC spectra. (Adapted with permission from Ref. [54]. Copyright 2015, American Chemical Society.).

Table 4
EXAFS Parameters of Y^{3+} in Na_xYF_{3+x} NCs. (Adapted with permission from Ref. [54]. Copyright 2015, American Chemical Society.).

Sample[a]	Shell	CN	Sample[a]	Shell	CN
S1	Y-F	7.1	F1	Y-F	6.9
S2	Y-F	7.7	F2	Y-F	7.3
S3	Y-F	7.9	F3	Y-F	7.9

[a] The molar ratio of [Na]/[RE] for samples of S1-S3, F1-F3 is 0.49, 0.73, 0.84, 0.48, 0.72 and 0.96, respectively.

parameters increased under otherwise identical synthesis conditions. Meanwhile, a slight increase of coordination number for Y^{3+} in Y-F shell was observed (Table 4), indicative of the distortion in the local environment around Ln^{3+} dopants. Furthermore, the overall UC emission of Er^{3+} in $Na_{0.5}YF_{3.5}$:Yb^{3+}/Er^{3+} NCs was revealed to be ~ 9 times stronger than that of $NaYF_4$:Yb^{3+}/Er^{3+} counterparts (Fig. 11). Likewise, a significant enhancement of UC red emission can be achieved by engineering the host composition. The ratio of red to green emission of Er^{3+} was observed to increase from 1.9 to 71 in Na_xYF_{3+x}:Yb^{3+}/Er^{3+} NCs when the ratio of [Na]/[RE] decreased from 0.96 to 0.48 [54]. Inspired by this work, Lin and co-workers synthesized nonstoichiometric Na_xYbF_{3+x}:Er^{3+} NCs *via* a facile solvothermal method [124]. With decreasing [Na]/[RE] and [F]/[RE] ratios, the UC emission intensity was gradually improved and red-to-green ratio increased as well, upon excitation at 915 nm. The enhanced UC emission and increased R/G ratio were attributed to the relatively high concentration of Na^+/F^- vacancies in the Na_xYbF_{3+x} host with low [Na]/[RE] ratio.

4. Conclusions

This review focuses on the site symmetry and optical properties of Ln^{3+}-doped disordered crystals. By using Ln^{3+} ions as spectroscopic probes and analyzing the high-resolution PL spectra, universal breakdown of crystallographic site symmetry has been revealed in a series of disordered crystals. Furthermore, the PL efficiency can be improved and the optical performance can be modulated *via* codoping Ln^{3+} with cations (homovalent or heterovalent ions) or engineering the host composition. As a result, a series of highly efficient Ln^{3+}-doped disordered phosphors were developed for diverse applications.

Despite the great advances in synthesis, charaterization and applications of Ln^{3+}-doped disordered crystals, there still many challenges remaining. On one hand, the microstructure of disordered crystals is much more complicated than that of ordered crystals. The optical spectroscopy characterization of Ln^{3+}-doped disordered crystals has to be complemented by other high-resolution structural characterization techniques (*e.g.*, scanning transmission electron microscope and electron energy-loss spectroscopy), which may provide direct microstructural information of the crystals. Only in this way, a correct and detailed description of Ln^{3+}-doped disordered crystals can be achieved. On the other hand, the relationship between local structure and optical properties of Ln^{3+} in disordered crystals is still not fully understood so far. More fundamental insights (*e.g.*, CF energy level fitting) are highly desired to identify the electronic energy levels and CF parameters in these Ln^{3+}-doped disordered phosphors, which is extremely important for clarification of the relationship between the microstructure and optical performance. Moreover, the results of CF energy level fitting might provide a useful guide to optimize the PL performance of Ln^{3+}-doped disordered crystals.

Acknowledgements

This work is supported by the Strategic Priority Research Program of the Chinese Academy of Sciences (XDB20000000 and XDA09030307), the 973 program of MOST (No. 2014CB845605), the NSFC (Nos. U1305244, 21325104, 21501180, 21650110462, 21771185, 11774345, and 51402294), the CAS/SAFEA International Partnership Program for Creative Research Teams, the Youth Innovation Promotion Association (No. 2014264), Fujian Provincial Natural Science Foundation (Nos. 2017I0018, 2017J01105, and 2017J05095), and the Chunmiao Project of Haixi Institutes of the CAS (No. CMZX-2014-003).

References

[1] Y. Zhang, L. Huang, X.G. Liu, Angew. Chem. Int. Ed. 55 (2016) 5718–5722.
[2] Y.H. Zhang, L.X. Zhang, R.R. Deng, J. Tian, Y. Zong, D.Y. Jin, X.G. Liu, J. Am. Chem. Soc. 136 (2014) 4893–4896.
[3] F. Wang, R.R. Deng, X.G. Liu, Nat. Protoc. 9 (2014) 1634–1644.
[4] B. Xiao, Y.S. Huang, L.Z. Zhang, Z.B. Lin, G.F. Wang, RSC Adv. 2 (2012) 5271–5276.
[5] N. Niu, F. He, S.L. Gai, C.X. Li, X. Zhang, S.H. Huang, P.P. Yang, J. Mater. Chem. C 22 (2012) 21613–21623.
[6] G.J. Wang, Y.S. Huang, L.Z. Zhang, S.P. Guo, G. Xu, Z.B. Lin, G.F. Wang, Cryst. Growth Des. 11 (2011) 3895–3899.
[7] C. Renero-Lecuna, R. Martín-Rodríguez, R. Valiente, J. González, F. Rodríguez, K.W. Kra¨mer, H.U. Gu¨del, Chem. Mater. 23 (2011) 3442–3448.
[8] Q. Liu, Y. Sun, T.S. Yang, W. Feng, C.G. Li, F.Y. Li, J. Am. Chem. Soc. 133 (2011) 17122–17125.
[9] P.I. Macfarlane, T.P.J. Han, B. Henderson, A.A. Kaminskii, Opt. Mater. 3 (1994) 15–24.
[10] X. Zhu, W. Feng, J. Chang, Y.W. Tan, J.C. Li, M. Chen, Y. Sun, F.Y. Li, Nat. Commun. 7 (2016) 10437.
[11] J.J. Peng, W. Xu, C.L. Teoh, S.Y. Han, B. Kim, A. Samanta, J.C. Er, L. Wang, L. Yuan, X.G. Liu, Y.T. Chang, J. Am. Chem. Soc. 137 (2015) 2336–2342.
[12] H. Dong, S.R. Du, X.Y. Zheng, G.M. Lyu, L.D. Sun, L.D. Li, P.Z. Zhang, C. Zhang, C.H. Yan, Chem. Rev. 115 (2015) 10725–10815.
[13] G.Y. Chen, H.L. Qiu, P.N. Prasad, X.Y. Chen, Chem. Rev. 114 (2014) 5161–5214.
[14] Y. Yang, Y. Sun, T.Y. Cao, J.J. Peng, Y. Liu, Y.Q. Wu, W. Feng, Y.J. Zhang, F.Y. Li, Biomaterials 34 (2013) 774–783.
[15] D.M. Yang, X.J. Kang, P.A. Ma, Y.L. Dai, Z.Y. Hou, Z.Y. Cheng, C.X. Li, J. Lin, Biomaterials 34 (2013) 1601–1612.
[16] H.T. Wong, M.K. Tsang, C.F. Chan, K.L. Wong, B. Fei, J.H. Hao, Nanoscale 5 (2013) 3465–3473.
[17] W. Feng, C.M. Han, F.Y. Li, Adv. Mater. 25 (2013) 5287–5303.
[18] J. Zhou, X.J. Zhu, M. Chen, Y. Sun, F.Y. Li, Biomaterials 33 (2012) 6201–6210.
[19] Y.M. Yang, Q. Shao, R.R. Deng, C. Wang, X. Teng, K. Cheng, Z. Cheng, L. Huang, Z. Liu, X.G. Liu, B.G. Xing, Angew. Chem. Int. Ed. 51 (2012) 3125–3129.
[20] A. Xia, M. Chen, Y. Gao, D.M. Wu, W. Feng, F.Y. Li, Biomaterials 33 (2012) 5394–5405.
[21] Y.F. Wang, L.D. Sun, J.W. Xiao, W. Feng, J.C. Zhou, J. Shen, C.H. Yan, Chem.-Eur. J. 18 (2012) 5558–5564.
[22] H.T. Wong, F. Vetrone, R. Naccache, H.L.W. Chan, J.H. Hao, J.A. Capobianco, J. Mater. Chem. B 21 (2011) 16589–16596.
[23] D.T. Tu, L.Q. Liu, Q. Ju, Y.S. Liu, H.M. Zhu, R.F. Li, X.Y. Chen, Angew. Chem. Int. Ed. 50 (2011) 6306–6310.
[24] Z.Q. Li, Y. Zhang, Angew. Chem. Int. Ed. 45 (2006) 7732–7735.
[25] C.X. Li, D.M. Yang, P.A. Ma, Y.Y. Chen, Y. Wu, Z.Y. Hou, Y.L. Dai, J.H. Zhao, C.P. Sui, J. Lin, Small 9 (2013) 4150–4159.
[26] P.A. Ma, H.H. Xiao, X.X. Li, C.X. Li, Y.L. Dai, Z.Y. Cheng, X.B. Jing, J. Lin, Adv. Mater. 25 (2013) 4898–4905.
[27] D.M. Yang, Y.L. Dai, P.G. Ma, X.J. Kang, Z.Y. Cheng, C.X. Li, J. Lin., Chem. -Eur. J. 19 (2013) 2685–2694.
[28] D.M. Yang, G.G. Li, X.J. Kang, Z.Y. Cheng, P.A. Ma, C. Peng, H.Z. Lian, C.X. Li, J. Lin, Nanoscale 4 (2012) 3450–3459.
[29] X. Zhang, P.P. Yang, Y.L. Dai, P.A. Ma, X.J. Li, Z.Y. Cheng, Z.Y. Hou, X.J. Kang, C.X. Li, J. Lin, Adv. Funct. Mater. 23 (2013) 4067–4078.
[30] P. Huang, D.T. Tu, W. Zheng, S.Y. Zhou, Z. Chen, X.Y. Chen, Sci. China Mater. 58 (2015) 156–177.
[31] Y. Liu, D.T. Tu, W. Zheng, L.Y. Lu, W.W. You, S.Y. Zhou, P. Huang, R.F. Li, X.Y. Chen, Nano Res. (2017), http://dx.doi.org/10.1007/s12274-017-1721-1.
[32] L.Y. Lu, D.T. Tu, Y. Liu, S.Y. Zhou, W. Zheng, X.Y. Chen, Nano Res. 11 (2017) 264–273.
[33] S. Lu, D.T. Tu, X.J. Li, R.F. Li, X.Y. Chen, Nano Res. 9 (2016) 187–197.
[34] X.W. Zhang, Z. Zhao, X. Zhang, D.B. Cordes, B. Weeks, B.S. Qiu, K. Madanan, D. Sardar, J. Chaudhuri, Nano Res. 8 (2015) 636–648.
[35] C. Cascales, A. Méndez Blas, M. Rico, V. Volkov, C. Zaldo, Opt. Mater. 27 (2005) 1672–1680.
[36] Y.K. Voron'ko, A.A. Sobol, S.N. Ushakov, V.E. Shukshin, Inorg. Mater.+ 38 (2002) 390–396.
[37] C. Feng, Z.J. Liu, Z.H. Cong, X.D. Xu, J. Xu, H. Rao, F. Bai, P. Li, Q.P. Wang, J.X. Fang, Chin. Opt. Lett. 14 (2016) 111402–111406.
[38] I. Mayer, S. Cohen, J. Solid State Chem. 48 (1983) 17–20.
[39] Y.S. Liu, W.Q. Luo, H.M. Zhu, X.Y. Chen, J. Lumin. 131 (2011) 415–422.
[40] W.Q. Luo, Y.S. Liu, X.Y. Chen, Sci. China Mater. 58 (2015) 819–850.
[41] A. Aebischer, M. Hostettler, J. Hauser, K. Kramer, T. Weber, H.U. Gudel, H.B. Burgi, Angew. Chem. Int. Ed. 45 (2006) 2802–2806.
[42] K. Binnemans, Coord. Chem. Rev. 295 (2015) 1–45.
[43] C.H. Yan, L.D. Sun, C.S. Liao, Y.X. Zhang, Y.Q. Lu, S.H. Huang, S.Z. Lü, Appl. Phys. Lett. 82 (2003) 3511–3513.
[44] Q. Ju, D.T. Tu, Y.S. Liu, R.F. Li, H.M. Zhu, J.C. Chen, Z. Chen, M.D. Huang, X.Y. Chen, J. Am. Chem. Soc. 134 (2012) 1323–1330.
[45] Q. Ju, Y.S. Liu, R.F. Li, L.Q. Liu, W.Q. Luo, X.Y. Chen, J. Phys. Chem. C 113 (2009) 2309–2315.
[46] D.T. Tu, Y.S. Liu, H.M. Zhu, R.F. Li, L.Q. Liu, X.Y. Chen, Angew. Chem. Int. Ed. 52 (2013) 1128–1133.
[47] D. Zakaria, M.T. Fournier, R. Mahiou, J.C. Cousseins, J. Alloy Compd. 188 (1992) 250–254.
[48] D. Zakaria, R. Mahiou, D. Avignant, M. Zahir, J. Alloy Compd. 257 (1997) 65–68.
[49] M. Karbowiak, J. Cichos, C. Rudowicz, Polyhedron 105 (2016) 42–48.
[50] M. Yang, H.P. You, Y.C. Jia, H. Qiao, N. Guo, Y.H. Song, CrystEngComm 13 (2011) 4046–4052.
[51] L.L. Li, L. Liu, W.W. Zi, H. Yu, S.C. Gan, G.J. Ji, H.F. Zou, X.C. Xu, J. Lumin. 143

(2013) 14–20.
[52] M.D. Wisser, S. Fischer, P.C. Maurer, N.D. Bronstein, S. Chu, A.P. Alivisatos, A. Salleo, J.A. Dionne, ACS Photonics 3 (2016) 1523–1530.
[53] H. Lin, D.K. Xu, D.D. Teng, S.H. Yang, Y.L. Zhang, Opt. Mater. 45 (2015) 229–234.
[54] H. Dong, L.D. Sun, Y.F. Wang, J. Ke, R. Si, J.W. Xiao, G.M. Lyu, S. Shi, C.H. Yan, J. Am. Chem. Soc. 137 (2015) 6569–6576.
[55] J. Zhou, Q. Liu, W. Feng, Y. Sun, F.Y. Li, Chem. Rev. 115 (2015) 395–465.
[56] W. Zheng, P. Huang, D.T. Tu, E. Ma, H.M. Zhu, X.Y. Chen, Chem. Soc. Rev. 44 (2015) 1379–1415.
[57] Y.I. Park, K.T. Lee, Y.D. Suh, T. Hyeon, Chem. Soc. Rev. 44 (2015) 1302–1317.
[58] X.M. Li, F. Zhang, D.Y. Zhao, Chem. Soc. Rev. 44 (2015) 1346–1378.
[59] X. Chen, D.F. Peng, Q. Ju, F. Wang, Chem. Soc. Rev. 44 (2015) 1318–1330.
[60] G.Y. Chen, H. Agren, T.Y. Ohulchanskyy, P.N. Prasad, Chem. Soc. Rev. 44 (2015) 1680–1713.
[61] Y.S. Liu, D.T. Tu, H.M. Zhu, X.Y. Chen, Chem. Soc. Rev. 42 (2013) 6924–6958.
[62] K.W. Krämer, D. Biner, G. Frei, H.U. Güdel, M.P. Hehlen, S.R. Lüthi, Chem. Mater. 16 (2004) 1244–1251.
[63] F. Wang, Y. Han, C.S. Lim, Y.H. Lu, J. Wang, J. Xu, H.Y. Chen, C. Zhang, M.H. Hong, X.G. Liu, Nature 463 (2010) 1061–1065.
[64] S.D. Liu, L.L. Dong, Y. Xu, X. Zhang, T.Q. Ren, X.D. Xu, Y.D. Peng, Y.P. Zhang, H.Y. Zhang, D.H. Li, B.T. Zhang, J.L. He, Appl. Opt. 55 (2016) 7659–7662.
[65] H.P. Ji, Z.H. Huang, Z.G. Xia, M.S. Molokeev, X.X. Jiang, Z.S. Lin, V.V. Atuchin, Dalton Trans. 44 (2015) 7679–7686.
[66] R. Yu, H.M. Noh, B.K. Moon, B.C. Choi, J.H. Jeong, K. Jang, S.S. Yi, J.K. Jang, J. Alloy Compd. 576 (2013) 236–241.
[67] P.A. Loiko, A.S. Yasukevich, A.E. Gulevich, M.P. Demesh, M.B. Kosmyna, B.P. Nazarenko, V.M. Puzikov, A.N. Shekhovtsov, A.A. Kornienko, E.B. Dunina, N.V. Kuleshov, K.V. Yumashev, J. Lumin. 137 (2013) 252–258.
[68] S. Georgescu, O. Toma, A.M. Chinie, L. Gheorghe, A. Achim, A.S. Stefan, Opt. Mater. 30 (2008) 1007–1012.
[69] H. Li, H.K. Yang, B.K. Moon, B.C. Choi, J.H. Jeong, K. Jang, H.S. Lee, S.S. Yi, Inorg. Chem. 50 (2011) 12522–12530.
[70] F.M. Emen, R. Altinkaya, J. Lumin. 134 (2013) 618–621.
[71] H.J. Seo, J. Alloy Compd. 604 (2014) 100–105.
[72] J.F. Suyver, J. Grimm, M.K. van Veen, D. Biner, K.W. Kramer, H.U. Gudel, J. Lumin. 117 (2006) 1–12.
[73] J.C. Boyer, F. Vetrone, L.A. Cuccia, J.A. Capobianco, J. Am. Chem. Soc. 128 (2006) 7444–7445.
[74] J.H. Zeng, J. Su, Z.H. Li, R.X. Yan, Y.D. Li, Adv. Mater. 17 (2005) 2119–2123.
[75] J.F. Suyver, J. Grimm, K.W. Kramer, H.U. Gudel, J. Lumin. 114 (2005) 53–59.
[76] S. Heer, K. Kompe, H.U. Gudel, M. Haase, Adv. Mater. 16 (2004) 2102–2105.
[77] P.H. Butler, Point Group Symmetry Application: Method and Tables, Plenum, New York, 1981.
[78] R. Liu, D.T. Tu, Y.S. Liu, H.M. Zhu, R.F. Li, W. Zheng, E. Ma, X.Y. Chen, Nanoscale 4 (2012) 4485–4491.
[79] Z.J. Wang, J.P. Zhong, H.B. Liang, J. Wang, Opt. Mater. Express 3 (2013) 418–425.
[80] F. Wang, J. Wang, X.G. Liu, Angew. Chem. Int. Ed. 49 (2010) 7456–7460.
[81] P. Huang, W. Zheng, S.Y. Zhou, D.T. Tu, Z. Chen, H.M. Zhu, R.F. Li, E. Ma, M.D. Huang, X.Y. Chen, Angew. Chem. Int. Ed. 53 (2014) 1252–1257.
[82] Q.L. Zou, P. Huang, W. Zheng, W.W. You, R.F. Li, D.T. Tu, J. Xu, X.Y. Chen, Nanoscale 9 (2017) 6521–6528.
[83] J.B. Zhao, D.Y. Jin, E.P. Schartner, Y.Q. Lu, Y.J. Liu, A.V. Zvyagin, L.X. Zhang, J.M. Dawes, P. Xi, J.A. Piper, E.M. Goldys, T.M. Monro, Nat. Nanotechnol. 8 (2013) 729–734.
[84] X.Y. Huang, Opt. Mater. Express 6 (2016) 2165–2176.
[85] G.T. Xiang, J.H. Zhang, Z.D. Hao, X. Zhang, Y.S. Luo, S.Z. Lü, H.F. Zhao, CrystEngComm 16 (2014) 2499–2507.
[86] M. Misiak, B. Cichy, A. Bednarkiewicz, W. Strek, J. Lumin. 145 (2014) 956–962.
[87] Z.Q. Liang, Y. Cui, S.L. Zhao, L.J. Tian, J.J. Zhang, Z. Xu, J. Alloy Compd. 610 (2014) 432–437.
[88] L. Lei, D.Q. Chen, J. Xu, R. Zhang, Y.S. Wang, Chem. Asian J. 9 (2014) 728–733.
[89] Y.L. Ding, X.D. Zhang, H.B. Gao, S.Z. Xu, C.C. Wei, Y. Zhao, J. Alloy Compd. 599 (2014) 60–64.
[90] V. Kale, T. Soukka, J. Holsa, M. Lastusaari, J. Nanopart. Res. 15 (2013) 1850.
[91] A. Aebischer, M. Hostettler, J. Hauser, K. Krämer, T. Weber, H.U. Güdel, H.B. Bürgi, Angew. Chem. Int. Ed. 45 (2006) 2802–2806.
[92] G. Huber, W. Lenth, J. Lieberts, F. Lutz, J. Lumin. 16 (1978) 353–360.
[93] H.M. Zhu, Y.J. Chen, Y.F. Lin, X.H. Gong, J.S. Liao, X.Y. Chen, Z.D. Luo, Y.D. Huang, J. Phys. D. Appl. Phys. 40 (2007) 6936–6941.
[94] H.M. Zhu, Y.F. Lin, Y.J. Chen, X.H. Gong, Q.G. Tan, Z.D. Luo, Y.D. Huang, J. Appl. Phys. 102 (2007) 063104.
[95] Y.F. Chen, H.C. Liang, J.C. Tung, K.W. Su, Y.Y. Zhang, H.J. Zhang, H.H. Yu, J.Y. Wang, Opt. Lett. 37 (2012) 461–463.
[96] F. Druon, S. Chenais, P. Raybaut, F. Balembois, P. Georges, R. Gaume, G. Aka, B. Viana, S. Mohr, D. Kopf, Opt. Lett. 27 (2002) 197–199.
[97] W. Zhao, W.W. Zhou, X.Y. Huang, G.F. Wang, Y. Yu, L.Y. Li, J.H. Huang, J.M. Du, H.J. Yu, Z.C. Lv, Y.H. Chen, J. Alloy Compd. 515 (2012) 74–79.
[98] A. Sarakovskis, G. Krieke, G. Doke, J. Grube, L. Grinberga, M. Springis, Opt. Mater. 39 (2015) 90–96.
[99] X.H. Chuai, X.Y. Guo, X.H. Liu, G.H. He, K.Z. Zheng, C.F. He, W.P. Qin, Opt. Mater. 44 (2015) 13–17.
[100] J.X. Fu, X.Z. Zhang, Z.C. Chao, Z.B. Li, J.S. Liao, D.J. Hou, H.R. Wen, X.N. Lu, X.R. Xie, Opt. Laser Technol. 88 (2017) 280–286.
[101] Q.M. Huang, J.C. Yu, E. Ma, K.M. Lin, J. Phys. Chem. C 114 (2010) 4719–4724.
[102] P. Ramasamy, P. Chandra, S.W. Rhee, J. Kim, Nanoscale 5 (2013) 8711–8717.
[103] Y.Q. Wu, S.B. Lin, W.Y. Shao, X.W. Zhang, J. Xu, L.W. Yu, K.J. Chen, RSC Adv. 6 (2016) 102869–102874.
[104] G.T. Xiang, J.H. Zhang, Z.D. Hao, X. Zhang, G.H. Pan, Y.S. Luo, H.F. Zhao, CrystEngComm 17 (2015) 3103–3109.
[105] Y.T. Zhang, Y.L. Shen, M. Liu, Y. Han, X.L. Mo, R.B. Jiang, Z.B. Lei, Z.H. Liu, F. Shi, W.P. Qin, CrystEngComm 19 (2017) 1304–1310.
[106] W. Zhu, Q.X. Wu, S.L. Zhao, Z.Q. Liang, Y.X. Yang, J.J. Zhang, Z. Xu, Opt. Mater. Express 6 (2016) 3001–3007.
[107] H.F. Zhou, X.C. Wang, Y.F. Lai, S.Y. Cheng, Q. Zheng, J.L. Yu, Appl. Phys. A-Mater. 123 (2017), http://dx.doi.org/10.1007/s00339-017-1260-3.
[108] D. Serrano, A. Braud, J.L. Doualan, P. Camy, R. Moncorgé, J. Opt. Soc. Am. B 29 (2012) 1854–1862.
[109] I.V. Gopich, A. Szabo, Proc. Natl. Acad. Sci. USA 109 (2012) 7747–7752.
[110] Q. Cheng, J.H. Sui, W. Cai, Nanoscale 4 (2012) 779–784.
[111] A. Dubey, A.K. Soni, A. Kumari, R. Dey, V.K. Rai, J. Alloy Compd. 693 (2017) 194–200.
[112] Y. Gao, Y.B. Hu, P. Ren, D.C. Zhou, J.B. Qiu, J. Rare Earth 33 (2015) 830–836.
[113] Y. Gao, Y.B. Hu, P. Ren, D.C. Zhou, J.B. Qiu, J. Alloy Compd. 667 (2016) 297–301.
[114] C.Z. Zhao, X.G. Kong, X.M. Liu, L.P. Tu, F. Wu, Y.L. Zhang, K. Liu, Q.H. Zeng, H. Zhang, Nanoscale 5 (2013) 8084–8089.
[115] S.W. Zhao, W. Liu, X.Y. Xue, Y.S. Yang, Z.Y. Zhao, Y.F. Wang, B. Zhou, RSC Adv. 6 (2016) 81542–81551.
[116] T. Cong, Y.D. Ding, J.P. Liu, H.Y. Zhao, X. Hong, Mater. Lett. 165 (2016) 59–62.
[117] W. Zheng, S.Y. Zhou, Z. Chen, P. Hu, Y.S. Liu, D.T. Tu, H.M. Zhu, R.F. Li, M.D. Huang, X.Y. Chen, Angew. Chem. Int. Ed. 52 (2013) 6671–6676.
[118] Y.B. Li, X.L. Li, Z.L. Xue, M.Y. Jiang, S.J. Zeng, J.H. Hao, Adv. Healthc. Mater. 6 (2017) 1601231.
[119] H. Yu, W.B. Cao, Q.M. Huang, E. Ma, X.Q. Zhang, J.C. Yu, J. Solid State Chem. 207 (2013) 170–177.
[120] D.Q. Chen, P. Huang, Y.L. Yu, F. Huang, A.P. Yang, Y.S. Wang, Chem. Commun. 47 (2011) 5801–5803.
[121] L. Lei, D.Q. Chen, P. Huang, J. Xu, R. Zhang, Y.S. Wang, Nanoscale 5 (2013) 11298–11305.
[122] M. Hu, D.D. Ma, Y.Z. Cheng, C.C. Liu, Z.P. Zhang, Y.J. Cai, S. Wu, R.F. Wang, J. Mater. Chem. B 5 (2017) 2662–2670.
[123] Z.Q. Liang, Y. Cui, S.L. Zhao, L.J. Tian, J.J. Zhang, Z. Xu, J. Alloy Compd. 610 (2014) 432–437.
[124] Y.N. Huang, Q.B. Xiao, H.S. Hu, K.C. Zhang, Y.M. Feng, F.J. Li, J. Wang, X.G. Ding, J. Jiang, Y.F. Li, L.Y. Shi, H.Z. Lin, Small 12 (2016) 4200–4210.